Identification of Chromatin Remodeling Genes *Arid4a* and *Arid4b* as Leukemia Suppressor Genes

Mei-Yi Wu, Karen W. Eldin, Arthur L. Beaudet

Background Leukemia evolves through a multistep process from premalignancy to malignancy. Epigenetic alterations, including histone modifications, have been proposed to play an important role in tumorigenesis. The involvement of two chromatin remodeling genes, retinoblastoma-binding protein 1 (*Rbbp1*/*Arid4a*) and *Rbbp1*-like 1 (*Rbbp1l1*/*Arid4b*), in leukemogenesis was not characterized.

Methods The leukemic phenotype of mice deficient for *Arid4a* with or without haploinsufficiency for *Arid4b* was investigated by serially monitoring complete blood counts together with microscopic histologic analysis and flow cytometric analysis of bone marrow and spleen from the $Arid4a^{-/-}$ mice or $Arid4a^{-/-}Arid4b^{+/-}$ mice. Regulation in bone marrow cells of downstream genes important for normal hematopoiesis was analyzed by reverse transcription–polymerase chain reaction. Genotypic effects on histone modifications were examined by western blotting and immunofluorescence analysis. All statistical tests were two-sided.

Results Young (2–5 months old) *Arid4a*-deficient mice had ineffective blood cell production in all hematopoietic lineages. Beyond 5 months of age, the $Arid4a^{-/-}$ mice manifested monocytosis, accompanied by severe anemia and thrombocytopenia. These sick $Arid4a^{-/-}$ mice showed bone marrow failure with myelofibrosis associated with splenomegaly and hepatomegaly. Five of 42 $Arid4a^{-/-}$ mice and 10 of 12 $Arid4a^{-/-}Arid4b^{+/-}$ mice progressed to acute myeloid leukemia (AML) and had rapid further increases of leukocyte counts. Expression of *Hox* genes (*Hoxb3*, *Hoxb5*, *Hoxb6*, and *Hoxb8*) was decreased in *Arid4a*-deficient bone marrow cells with or without *Arid4b* haploinsufficiency, and *FoxP3* expression was reduced in $Arid4a^{-/-}Arid4b^{+/-}$ bone marrow. Increases of histone trimethylation of H3K4, H3K9, and H4K20 (fold increases in trimethylation = 32, 95% confidence interval [CI] = 27 to 32; 45, 95% CI = 41 to 49; and 2.2, 95% CI = 1.7 to 2.7, respectively) were observed in the bone marrow of *Arid4a*-deficient mice.

Conclusions *Arid4a*-deficient mice initially display ineffective hematopoiesis, followed by transition to chronic myelomonocytic leukemia (CMML)–like myelodysplastic/myeloproliferative disorder, and then transformation to AML. The disease processes in the *Arid4a*-deficient mice are very similar to the course of events in humans with CMML and AML. This mouse model has the potential to furnish additional insights into the role of epigenetic alterations in leukemogenesis, and it may be useful in developing novel pharmacological approaches to treatment of preleukemic and leukemic states.

J Natl Cancer Inst 2008;100:1247–1259

The human *ARID4A* and *ARID4B* genes, previously known as retinoblastoma-binding protein 1 (*RBBP1*, *RBP1*) (1,2) and *RBBP1*–like protein 1 (*RBBP1L1*) (3), respectively, are homologous members of the AT-rich interaction domain (*ARID*) gene family (4). The ARID4A amino acid sequence, but not that of ARID4B, contains an LVCHE sequence as a conserved LXCXE motif known to interact with the pocket of retinoblastoma protein (RB) (1,2). We reported that ARID4A interacts with ARID4B (5). Both ARID4A and ARID4B contain a Tudor domain, an ARID domain, and a chromodomain (4), as well as two repression domains, R1 and R2, with part of the R1 domain overlapping the ARID domain (6). The ARID domain contains a helix-turn-helix structure with DNA binding activity (7). Chromodomains are found in a variety of proteins that play roles in the functional organization of chromosome structure through chromatin remodeling (8–10). Both chromodomains and Tudor domains mediate binding to methylated lysines of histones H3 and H4 (11–14). ARID4A recruited by RB has been defined as a repressor of E2F-dependent transcription (15). Through their R2 regions, ARID4A and ARID4B serve as adapters to recruit the mSin3A–histone deac-

Affiliations of authors: Department of Molecular and Human Genetics, Baylor College of Medicine (MYW, ALB) and Department of Pathology, Baylor College of Medicine, Texas Children's Hospital (KWE), Houston, TX.

Correspondence to: Arthur L. Beaudet, MD, Department of Molecular and Human Genetics, Baylor College of Medicine, One Baylor Plaza, Houston, TX 77030 (e-mail: abeaudet@bcm.edu).

See "Funding" and "Notes" following "References."

DOI: 10.1093/jnci/djn253

CONTEXT AND CAVEATS

Prior knowledge

Epigenetic modifications of DNA have been proposed to play an important role in carcinogenesis. The involvement of two chromatin remodeling genes, *Arid4a* and *Arid4b*, in the etiology of leukemia was unknown.

Study design

Mice deleted for *Arid4a* or mice deleted for *Arid4a* and haploinsufficient for *Arid4b* were characterized in terms of blood counts, bone marrow abnormalities as revealed by histologic analysis, gene transcription, and epigenetic modification in their bone marrow cells.

Contribution

The fact that the genetically modified mice progressed to acute myeloid leukemia suggests a critical role for epigenetic modifications mediated by *Arid4a and Arid4a* in suppression of leukemogenesis.

Implications

The mouse model described here may be useful for studying the etiology of leukemia and the role that epigenetic modification plays in this process.

Limitations

The suitability of the mouse strains described here as a model for human leukemia and the precise roles of *Arid4a* and *Arid4b* in chromatin remodeling remain to be determined.

From the Editors

etylase (HDAC) histone-modifying complex to E2F-dependent promoters (6,16,17). ARID4A and ARID4B also provide a repressive function in an HDAC-independent manner through their R1 regions. Transcriptional repression activity via the R1 region is controlled by SUMOylation, a posttranslational modification by small ubiquitin-related modifier proteins (18).

Several lines of evidence suggest that ARID4A and ARID4B may be involved in the pathogenesis of breast and other cancers. RB (with which ARID4A interacts and which is inactivated in many tumors) has been shown to be involved in many cellular processes, including control of the cell cycle, cell differentiation, DNA-damage responses, DNA replication, and protection against apoptosis (19). Repression of E2F-dependent transcription by ARID4A and ARID4B in conjunction with RB leads to cell arrest reminiscent of senescence (15,18). Screening a cDNA library from the MCF7 breast cancer cell line with IgG purified from the serum of a breast cancer patient identified ARID4A and ARID4B as tumor-associated antigens, and breast cancer patients have high titers of antibodies against both proteins (3,20,21). Furthermore, human cytotoxic T cells stimulated with ARID4A peptides kill breast cancer cells (22). ARID4A also interacts with the breast cancer metastasis suppressor 1 (BRMS1) and the BRMS1 homologue p40 in the mSin3–HDAC complex (23,24). BRMS1 reduces the metastatic activity of cancer cells without affecting tumorigenicity (25). Despite these reports, the role of ARID4A and ARID4B in cancer development is unclear.

Preleukemic conditions are relatively common in aging populations, and little is known about their pathogenesis or how they predispose to leukemia. Many physicians and patients face this distressing clinical situation on a chronic basis, and there is little that the physician can offer to prevent the potential transformation to malignancy because the mechanisms by which cancer progresses from premalignancy to malignancy are not fully understood.

Epigenetic alterations such as histone modifications of chromatin structure have been suggested to be involved in the development of leukemia and other cancers (26). Although an increasing number of chromatin remodeling proteins have been defined biochemically (27), their biological functions, particularly in the context of an animal model, are poorly characterized, and the molecular events governing chromatin reorganization in cancer cells remain relatively unexplored. Recently, we developed mouse models for *Arid4a* and *Arid4b* deficiency that demonstrated the function of *Arid4a* and *Arid4b* in the regulation of genomic imprinting through control of epigenetic modifications (5). Here, we use these mouse models deficient for *Arid4a*, alone or in combination with haploinsufficiency for *Arid4b*, to analyze a premalignant hematopoietic disorder and eventual leukemia.

Methods

Animal Care

The mice (100 wild-type mice, 150 *Arid4a*$^{-/-}$ mice, 40 *Arid4a*$^{+/-}$*Arid4b*$^{+/-}$ mice, and 40 *Arid4a*$^{-/-}$*Arid4b*$^{+/-}$ mice) were all bred and maintained according to a protocol approved by the Baylor College of Medicine Animal Care and Use Committee at the institution's specific pathogen–free mouse facility, which is approved by the American Association for Accreditation of Laboratory Animal Care and is operated in accordance with current regulations and standards of the US Departments of Agriculture and of Health and Human Services.

Beginning at 5 months of age, the *Arid4a*$^{-/-}$ mice and *Arid4a*$^{-/-}$*Arid4b*$^{+/-}$ mice were monitored weekly for signs of morbidity. Blood was obtained weekly for complete blood cell counts. Mice were sacrificed when they met any of the following criteria: 1) obvious morbidity, in which case mice proved to have either severe anemia or greatly increased white blood cell (WBC) counts; 2) severe anemia or high WBC counts with milder or impending morbidity; or 3) marked splenomegaly or hepatomegaly. Mice were anesthetized with isoflurane and then killed by cervical dislocation. The mice were dissected, and organs were examined for the presence or absence of tumor enlargement. The lung, spleen, and liver were removed, and bone marrow cells from both femurs were flushed with syringes.

Hematologic Analysis

Mice (52 wild-type mice, 50 *Arid4a*$^{-/-}$ mice, 40 *Arid4a*$^{+/-}$*Arid4b*$^{+/-}$ mice, and 10 *Arid4a*$^{-/-}$*Arid4b*$^{+/-}$ mice) were anesthetized with isoflurane, and blood from each mouse was obtained from the retro-orbital venous plexus. Complete blood cell counts were determined with an analyzer (ADVIA 120 Hematology System; Bayer Diagnostics).

Peripheral blood and bone marrow smears were stained with Wright–Giemsa stain. On the peripheral blood smears (from 10 wild-type mice, more than 20 chronic myelomonocytic leukemia [CMML]–like *Arid4a*$^{-/-}$ mice, three acute myeloid leukemia [AML] *Arid4a*$^{-/-}$ mice, and five AML *Arid4a*$^{-/-}$*Arid4b*$^{+/-}$ mice) and bone marrow smears (from five wild-type mice, five CMML-like *Arid4a*$^{-/-}$ mice, two AML *Arid4a*$^{-/-}$ mice, and three AML *Arid4a*$^{-/-}$ *Arid4b*$^{+/-}$ mice), we analyzed blasts, immature precursors, WBCs (including lymphocytes, neutrophils, monocytes, eosinophils, and basophils), red blood cells (RBCs), and platelets.

Histologic Analysis

For bone marrow examination, femurs from three wild-type mice and three *Arid4a*$^{-/-}$ mice were fixed and decalcified by immersion in Cal-EXII solution (Fisher Scientific, Pittsburgh, PA). Spleen and liver from five wild-type mice, five CMML-like mice, and five AML mice were fixed in 10% formalin (Fisher Scientific). Histology was performed on 5-μm paraffin-embedded tissue sections that were stained either with reticulin to show myelofibrosis for femur bone sections (three slides from three wild-type mice and three slides from three *Arid4a*$^{-/-}$ mice) or with hematoxylin and eosin to show extramedullary hematopoiesis in spleen and liver (one slide each from five wild-type mice, five CMML-like *Arid4a*$^{-/-}$ mice, and five AML *Arid4a*$^{-/-}$*Arid4b*$^{+/-}$ mice).

Flow Cytometry

Spleens were removed from mice and dissociated into single cells by sliding tissue between two superfrost microscope slides. RBCs were lysed by hypotonic buffer (NH_4Cl, 0.14 *M*; Tris, 0.017 *M*, pH 7.2). Cells from spleen or bone marrow were gently filtered through 70-μm cell strainers (BD Falcon, VWR, Batavia, IL) and were stained with directly fluorescein-5-isothiocyanate (FitC)-conjugated antibodies to c-kit (2B8, eBioscience, San Diego, CA), Sca1 (D7, eBioscience), Mac1 (M1/70, BD Biosciences Pharmingen, San Jose, CA), Gr1 (RB6-8C5, BD Biosciences Pharmingen), B220 (RA3-6B2, BD Biosciences Pharmingen), CD19 (1D3, BD Biosciences Pharmingen), CD3 (145-2C11, BD Biosciences Pharmingen), or Ter119 (Ter119, eBioscience). A lineage antibody cocktail (Lin) included antibodies against Mac1 (M1/70), Gr1 (RB6-8C5), CD4 (L3T4, BD Biosciences Pharmingen), CD8 (53-6.7, BD Biosciences Pharmingen), CD19 (1D3), and B220 (RA3-6B2) to stain bone marrow cells. All antibodies were diluted (1:100) in phosphate-buffered saline (PBS). Hematopoietic stem cells (HSCs) ($Lin^{-}Sca1^{+}c\text{-}Kit^{+}$), common myeloid progenitors (CMPs) ($Lin^{-}Sca1^{-}c\text{-}Kit^{+}$), granulocytes and monocytes ($Gr1^{+}Mac1^{+}$), erythroid cells ($Ter119^{+}$), T cells ($CD3^{+}$), and B cells ($B220^{+}CD19^{+}$) were analyzed. For apoptosis analysis, bone marrow cells were stained with annexin V–FITC conjugates (BD Biosciences Pharmingen). Cells were then washed and analyzed by flow cytometry (Beckman-Coulter EPICS XL-MCL).

Immunofluorescence

Bone marrow cells flushed from femur bones were fixed in 4% paraformaldehyde, spread on glass slides, and permeabilized in cold acetone. Subsequently, cells were blocked with 5% bovine serum albumin in PBS, followed by incubation with primary antibodies against trimethylated H3K9, H3K4, or H4K20 (07-442 for H3K9me3, 05-745 for H3K4me3, and 07-463 for H4K20me3, Upstate, Charlottesville, VA) at a dilution of 1:200 in blocking solution. Then, cells were washed with blocking solution and incubated with Alexa 488–conjugated goat anti–rabbit secondary antibody (Molecular Probes, Invitrogen, Carlsbad, CA). Cells were mounted with Vectashield containing 4',6-diamidino-2-phenylindole (DAPI) (Vector Laboratories, Burlingame, CA) and analyzed on a deconvolution fluorescence microscope (DeltaVision Restoration Microscope, Zeiss, Jena, Germany).

Western Blotting

Bone marrow cells flushed from femurs were resuspended in lysis buffer (10 m*M* HEPES, pH 7.9, 1.5 m*M* $MgCl_2$, 10 m*M* KCl, and protease inhibitors [Complete protease inhibitor cocktail tablets, Roche, Indianapolis, IN]). Histones were acid extracted by 0.2 N HCl and precipitated with 20% trichloroacetic acid. Proteins were electrophoresed on 7.5% Tris–Cl ready gels (Bio-Rad, Hercules, CA) and then transferred to nitrocellulose membranes (Bio-Rad). The incubations with the appropriate primary antibodies were performed as follows: rabbit anti-H3 (1:1000 dilution, ab1791, Abcam, Cambridge, MA), goat anti-H4 (1:100 dilution, sc-8658, Santa Cruz Biotechology, Santa Cruz, CA), rabbit anti-H2AX (1:5000 dilution, BL179, Bethyl, TX), rabbit anti-H3K4me3 (1:4000 dilution, 05-745, Upstate), rabbit anti-H3K9me3 (1:500 dilution, 07-523, Upstate), or rabbit anti-H4K20me3 (1:200 dilution, 07-749, Upstate). The membranes were then incubated with either goat anti–rabbit IgG horseradish peroxidase (HRP) (1:5000 dilution, ac-2004, Santa Cruz Biotechnology) or donkey anti–goat HRP (1:5,000 dilution, ac-2020, Santa Cruz Biotechnology). Antibody binding was detected by enhanced chemiluminesence (ECL, Amersham, Piscataway, NJ).

Reverse Transcription–Polymerase Chain Reaction

Total RNA was purified from bone marrow cells using an RNeasy plus kit (Qiagen, Hilden, Germany). Total RNA (5 μg) was used for reverse transcription to synthesize the first-strand cDNA (Superscript III First-strand synthesis system, Invitrogen). cDNA (5 μg) was used for polymerase chain reaction (PCR). PCR conditions and primer sequences have been described (28) and/or are listed in Supplementary Table 1, available online. Hprt transcripts were amplified as a control for gene expression.

Statistical Analysis

Means and the accompanying 95% confidence intervals were calculated from at least three independent experiments. Group means were compared using a two-sided Student *t* test. *P* values less than .05 were considered to be statistically significant.

Results

A CMML-like Myelodysplastic/Myeloproliferative Disorder in *Arid4a*-Deficient Mice

To investigate the function of *Arid4a* and *Arid4b*, we bred *Arid4a* null (*Arid4a*$^{-/-}$) mice and mice null for *Arid4a* and heterozygous for the *Arid4b* deletion (*Arid4a*$^{-/-}$*Arid4b*$^{+/-}$); homozygous null mutants for *Arid4b* (both *Arid4a*$^{+/+}$*Arid4b*$^{-/-}$ and *Arid4a*$^{-/-}$*Arid4b*$^{-/-}$) were not viable and died before E7.5 (5). Young (2–5 months old) adult *Arid4a*-deficient mice initially had ineffective blood cell production in all hematopoietic lineages, with mild leukopenia (WBC: mean wild-type count = 7.64×10^6/mL, mean *Arid4a*$^{-/-}$ count = 4.09×10^6/mL, difference = 3.55×10^6/mL, 95% confidence interval [CI] = 2.72×10^6/mL to 4.38×10^6/mL, $P < .001$. Lymphocyte: mean wild-type count = 6.29 × 10^6/mL, mean *Arid4a*$^{-/-}$ count = 3.21 × 10^6/mL, difference = 3.08 × 10^6/mL, 95% CI = 2.22 × 10^6/mL to 3.94 × 10^6/mL, $P < .001$. Neutrophil: mean wild-type count = 0.84 × 10^6/mL, mean *Arid4a*$^{-/-}$ count = 0.51 × 10^6/mL, difference = 0.33 × 10^6/mL, 95% CI = 0.16 × 10^6/mL to 0.51 × 10^6/mL, $P = .043$) and mild anemia (RBC: mean wild-type count = 8.96 × 10^9/mL, mean *Arid4a*$^{-/-}$ count = 7.88 × 10^9/mL, difference = 1.08 × 10^9/mL, 95% CI = 0.5 × 10^9/mL to 1.66 × 10^9/mL, $P = .017$; hemoglobin: mean wild-type count = 137.8 g/L, mean *Arid4a*$^{-/-}$ count = 125.0 g/L, difference = 12.8 g/L, 95% CI = 5.0 g/L to 20.7 g/L, $P = .035$) with statistically significant thrombocytopenia (platelet: mean wild-type count = 1144.3 × 10^6/mL, mean *Arid4a*$^{-/-}$ count = 225.8 × 10^6/mL, difference = 918.5 × 10^6/mL, 95% CI = 802.3 × 10^6/mL to 1034.7 × 10^6/mL, $P < .001$) (Figure 1, A). Beyond 5 months of age, the *Arid4a*$^{-/-}$ mice manifested monocytosis (monocyte: mean wild-type count = 0.2 × 10^6/mL, mean *Arid4a*$^{-/-}$ count = 0.9 × 10^6/mL, difference = 0.7 × 10^6/mL, 95% CI = 0.55 × 10^6/mL to 0.85 × 10^6/mL, $P < .001$), accompanied with severe anemia (RBC: mean wild-type count = 8.6 × 10^9/mL, mean *Arid4a*$^{-/-}$ count = 3.1 × 10^9/mL, difference = 5.5 × 10^9/mL, 95% CI = 5.0 × 10^9/mL to 6.0 × 10^9/mL, $P < .001$; hemoglobin: mean wild-type count = 130 g/L, mean *Arid4a*$^{-/-}$ count = 48 g/L, difference = 82 g/L, 95% CI = 76 g/L to 88 g/L, $P < .001$) and severe thrombocytopenia (platelet: mean wild-type count = 1169 × 10^6/mL, mean *Arid4a*$^{-/-}$ count = 76 × 10^6/mL, difference = 1093 × 10^6/mL, 95% CI = 1036 × 10^6/mL to 1150 × 10^6/mL, $P < .001$) (Figure 1, A). Peripheral blood smears from older (more than 5 months old) sickly *Arid4a*$^{-/-}$ mice showed the presence of teardrop poikilocytes (Figure 1, B, a) and increased numbers of immature erythroid cells (Figure 1, B, b and c). Immature and maturing mononuclear cells morphologically consistent with the monocyte lineage were also noted in the peripheral blood (Figure 1, B, d). Some monocytoid cells that contained phagocytosed RBCs were also present (Figure 1, B, e). The *Arid4a*$^{-/-}$ mice showed signs of morbidity (eg, ruffled hair, decreased activity, and rapid respiration). Mortality of the *Arid4a*$^{-/-}$ mice increased sharply from 6 months of age onward, with no *Arid4a*$^{-/-}$ mice surviving past 22 months of age (Figure 1, C). Increased mortality appeared to be associated with increasing severity of the hematologic abnormalities, especially severe anemia, in *Arid4a*$^{-/-}$ mice.

Bone marrow from sick *Arid4a*$^{-/-}$ mice developing monocytosis and severe anemia in the peripheral blood showed reticulin fibrosis and an increased number (average increase = 8%, 95% CI = 6% to 10%, $P < .001$; the 10.9% increase in Figure 1, E is from one of five separate experiments) of apoptotic cells compared with wild-type mice (Figure 1, D and E). The sick *Arid4a*$^{-/-}$ mice (n > 50) also developed splenomegaly (Figure 1, F) and hepatomegaly (Figure 1, G) after 5 months of age, with extramedullary hematopoiesis in the spleen (Figure 1, H) and liver (Figure 1, I). A marked increase of erythropoiesis within enlarged spleens of the *Arid4a*$^{-/-}$ mice was demonstrated by flow cytometry analysis of spleen cells: 65% of spleen cells were erythroid cells (Ter119$^+$) in mutants versus 7% in wild-type mice (difference = 58%, 95% CI = 53% to 63%, $P < .001$) (Figure 1, J).

In addition to their hematologic abnormalities, female *Arid4a*$^{-/-}$ mice showed decreased fertility. Litter sizes for the *Arid4a*$^{-/-}$ females mating with wild-type males were markedly lower than those for wild-type breeding pairs (0.7 vs 7.8, difference = 5.6, 95% CI = 5.2 to 6.0. $P < .001$). Anemia, hepatosplenomegaly, and systemic illness may have contributed to the decreased fertility, but in addition there was hemorrhage into the ovarian follicles (Supplementary Figure 1, available online), as a result of profound thrombocytopenia (the mean platelet count in these mice was less than 100 × 10^6/mL, Figure 1, A).

Thus, *Arid4a*$^{-/-}$ mice initially developed mild cytopenias with substantial thrombocytopenia and later progressed to monocytosis associated with more severe anemia and thrombocytopenia with spontaneous hemorrhage into organs (ie, ovary). Bone marrow failure with myelofibrosis was associated with hepatosplenomegaly due to compensatory extramedullary hematopoiesis. These abnormalities in the *Arid4a*$^{-/-}$ mice suggest a myelodysplastic/myeloproliferative disorder and are similar to the course of events in humans with CMML derived from myelodysplastic/myeloproliferative diseases.

Development of AML in *Arid4a*$^{-/-}$ Mice and *Arid4a*$^{-/-}$*Arid4b*$^{+/-}$ Mice

In patients with myelodysplastic/myeloproliferative diseases, progression to AML occurs with a frequency of 5%–30%. Similarly, we found that 5 of 42 (12%) of the *Arid4a*$^{-/-}$ mice developed AML showing rapid and large increases of WBC counts with an onset between 12 and 22 months of age (data not shown). Hematologic malignancies were more frequent in the *Arid4a*$^{-/-}$*Arid4b*$^{+/-}$ mice. Of the 12 *Arid4a*$^{-/-}$*Arid4b*$^{+/-}$ mice monitored beyond 5 months of age, 10 (83%) developed AML with an earlier age of onset (7–15 months).

Neither the mice heterozygous for both Arid4a and Arid4b (n = 36) nor wild-type controls (n = 52) developed AML over a 2-year period. littermates (data not shown). Postnatal growth was also delayed (Figure 2, A); body weight of *Arid4a*$^{-/-}$*Arid4b*$^{+/-}$ mice was 30% less than that of wild-type mice at 7 weeks of age (Figure 2, B). The *Arid4a*$^{-/-}$*Arid4b*$^{+/-}$ mice also had increased postnatal mortality: 25% of mutant mice died before attaining 1 month of age (Figure 2, C), and those that survived exhibited increased mortality at 7 months of age (Figure 2, C) that was attributable to the increasing severity of their hematologic malignancies.

Bone marrow smears from mice with AML (two *Arid4a*$^{-/-}$ mice and three *Arid4a*$^{-/-}$*Arid4b*$^{+/-}$ mice) demonstrated the presence of a mixture of immature and dysplastic WBC precursors with more than 20% nonlymphoid immature forms and blasts (Figure 3, A). Flow cytometric analysis of cell populations within the bone marrow from the *Arid4a*$^{-/-}$ mice with CMML-like phenotype and the *Arid4a*$^{-/-}$*Arid4b*$^{+/-}$ mice with AML revealed that the majority of excess leukocytes were granulocytes and monocytes (22% of wild-type mice, 29% of mice with CMML-like phenotype, and 63% of mice with AML were positive for Gr1 and Mac1, difference between wild-type and CMML-like mice = 7%, $P = .124$; difference between wild-type and AML mice = 41%, $P = .002$) (Figure 4, A). This increase in granulocytes and monocytes was accompanied by an increase of T lymphoid cells (CD3$^+$, 0.65% T lymphoid cells in wild-type mice, 3.16% in mice with CMML-like phenotype, and 5.99% in AML mice, difference between wild-type and CMML-like mice = 2.15%, $P = .029$; difference between wild-type and AML mice = 5.34%, $P < .001$) and by decreases in B lymphoid cells (B220$^+$CD19$^+$, 9.4% in wild-type mice, 1.8% in mice

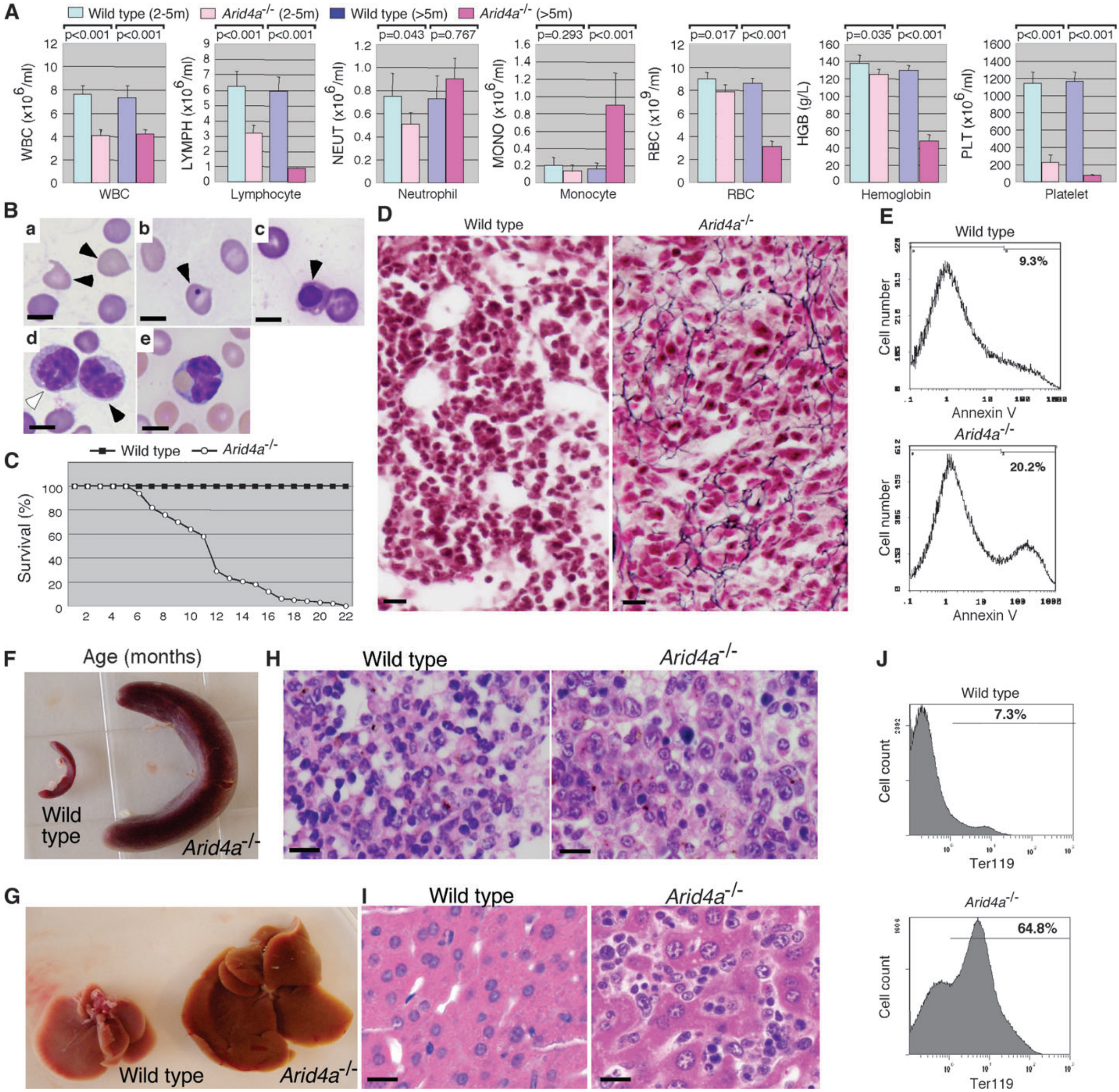

Figure 1. A chronic myelomonocytic leukemia (CMML)–like myelodysplastic/myeloproliferative disorder in *Arid4a*-deficient mice. **A**) Complete blood counts (white blood cell, lymphocyte, neutrophil, monocyte, red blood cell [RBC], hemoglobin, platelet) in wild-type mice at 2–5 months of age (n = 35), in *Arid4a*$^{-/-}$ mice at 2–5 months of age (n = 30), in wild-type mice more than 5 months old (n = 25), and in *Arid4a*$^{-/-}$ mice more than 5 months old with symptoms of CMML (n = 25). Means (and 95% confidence intervals) for cell concentrations are shown, and *P* values were calculated using Student *t* test. **B**) Wright–Giemsa staining of peripheral blood from an *Arid4a*$^{-/-}$ mouse with symptoms of CMML, showing teardrop poikilocytes (a, **black arrowheads**), red cells with Howell–Jolly bodies (b, **black arrowhead**), and nucleated red cells (c, **black arrowhead**). Immature (d, **white arrowhead**) and maturing (d, **black arrowhead**) mononuclear cells were also observed, together with phagocytosis of RBC by a monocyte (e, **arrowhead**). Ten separate analyses were performed. **Scale bars** = 5 µm. **C**) Survival of *Arid4a*$^{-/-}$ (n = 25) mice and wild-type (n = 25) mice. **D**) Reticulin staining of paraffin sections of bone marrow from a wild-type mouse and a sick *Arid4a*$^{-/-}$ mouse. The *Arid4a*$^{-/-}$ sample shows fibrous tissue stained with black color. Scale bars = 20 µm. **E**) Flow cytometric analysis of apoptotic cells in bone marrow from a wild-type and a sick *Arid4a*$^{-/-}$ mouse. The percentages of cells positive for annexin V are indicated. Five separate cytometric analyses were performed. **F**) Splenomegaly and **G**) hepatomegaly in a sick *Arid4a*$^{-/-}$ mouse. Hematoxylin and eosin–stained sections of **H**) spleen and **I**) liver from a wild-type mouse and a sick *Arid4a*$^{-/-}$ mouse. Extramedullary hematopoiesis was found in the *Arid4a*$^{-/-}$ spleen and *Arid4a*$^{-/-}$ liver, which were infiltrated with nucleated elements of blood cells. Ten separate analyses were performed. Scale bars = 20 µm. **J**) Flow cytometric analysis of cells from spleen in a wild-type mouse and an *Arid4a*$^{-/-}$ mouse stained with Ter119 surface antigen. The percentages of cells positive for the antigen are indicated. Twenty separate analyses were performed.

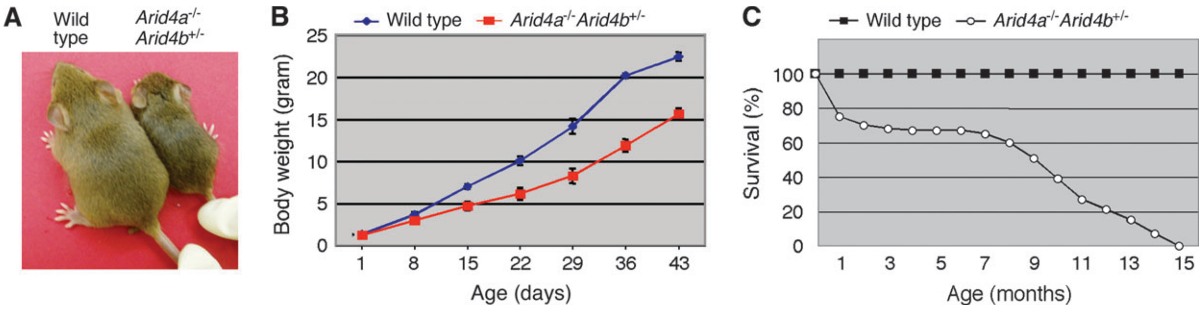

Figure 2. Growth and survival of the *Arid4a*$^{-/-}$*Arid4b*$^{+/-}$ mice. **A**) Growth retardation in an *Arid4a*$^{-/-}$*Arid4b*$^{+/-}$ mouse compared with a wild-type littermate at 12 days of age. **B**) Growth curve of the *Arid4a*$^{-/-}$*Arid4b*$^{+/-}$ (n = 7) and wild-type (n = 10) littermates by mean body weight plotted against age with 95% confidence intervals. **C**) Survival of *Arid4a*$^{-/-}$*Arid4b*$^{+/-}$ (n = 31) and wild-type (n = 25) mice.

with CMML-like phenotype, and 0.9% in AML mice, difference between wild-type and CMML-like mice = 7.6%, $P < .001$; difference between wild-type and AML mice = 8.5%, $P < .001$) and erythroid populations (Ter119$^+$, 60% erythroid cells in wild-type mice, 54% in mice with CMML-like phenotype, and 36% in AML mice, difference between wild-type and CMML-like mice = 6%, $P = .378$; difference between wild-type and AML mice = 24%, $P = .026$) (Figure 4, A).

Examination of peripheral blood smears from the *Arid4a*$^{-/-}$ and *Arid4a*$^{-/-}$*Arid4b*$^{+/-}$ mice with AML showed the presence of more than 20% of atypical cells with morphology consistent with blasts or immature myeloid precursors (Figure 3, B, a–d). There was accompanying monocytosis, and hemophagocytosis was often observed (Figure 3, B, e). Serial monitoring of peripheral blood counts in mice developing AML revealed a rapid increase of WBC counts over a 2- to 4-week interval. The elevated WBC count was attributable to increased neutrophilic and monocytic forms (neutrophil: mean wild-type count = 0.75×10^6/mL, mean AML count = 8.50×10^6/mL, difference = 7.75×10^6/mL, 95% CI = 5.85×10^6/mL to 9.65×10^6/mL, $P < .001$; monocyte: mean wild-type count = 0.16×10^6/mL, mean AML count = 3.90×10^6/mL, difference = 3.74×10^6/mL, 95% CI = 2.54×10^6/mL to 4.94×10^6/mL, $P < .001$) (Figure 4, A). Soon after the development of leukocytosis, the mice became moribund and were sacrificed. In most of the *Arid4a*$^{-/-}$*Arid4b*$^{+/-}$ mice, AML occurred before development of severe anemia (peripheral blood in Figure 4, A; hemoglobin: mean wild-type count = 130 g/L, mean *Arid4a*$^{-/-}$*Arid4b*$^{+/-}$ count = 71 g/L, difference = 59 g/L, 95% CI = 40 g/L to 78 g/L, $P < .001$). Of the few *Arid4a*$^{-/-}$ mice that progressed to AML, most developed a CMML-like phenotype and became moribund from severe anemia (hemoglobin: mean wild-type count = 130 g/L, mean *Arid4a*$^{-/-}$ count = 48 g/L, difference = 82 g/L, 95% CI = 76 g/L to 88 g/L, $P < .001$) (Figures 1, A and 4, A).

Development of Myeloid Sarcoma in *Arid4a*$^{-/-}$ and *Arid4a*$^{-/-}$*Arid4b*$^{+/-}$ Mice

In the human World Health Organization classification (29), myeloid sarcoma is considered an alternative presentation of AML. The *Arid4a*$^{-/-}$ mice and the *Arid4a*$^{-/-}$*Arid4b*$^{+/-}$ mice with leukemia also developed myeloid sarcoma. Soft tissue tumor nodules were found within the enlarged spleens (Figure 5, A) and livers (Figure 5, B) that were infiltrated with aggressive leukemic (malignant) cells

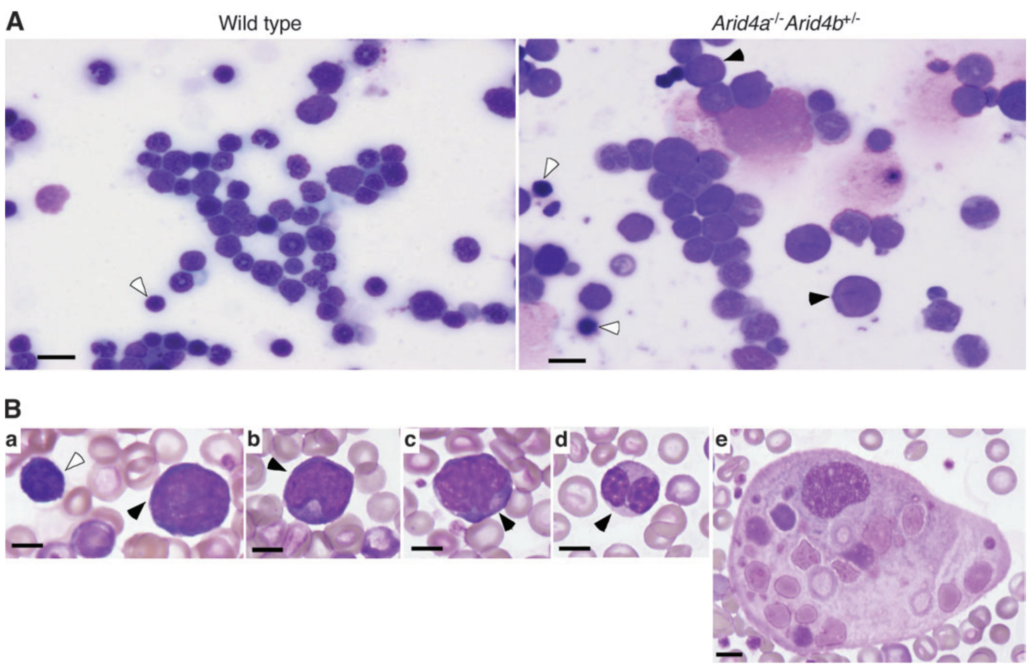

Figure 3. Acute myeloid leukemia (AML)–like phenotype in *Arid4a*$^{-/-}$*Arid4b*$^{+/-}$ mice. **A**) Bone marrow smears from a wild-type mouse and an *Arid4a*$^{-/-}$*Arid4b*$^{+/-}$ mouse with AML were stained with Wright–Giemsa. **Black arrowheads** indicate blasts. **White arrowheads** indicate red blood cell precursors in both wild-type and AML bone marrow (for both wild-type and the *Arid4a*$^{-/-}$*Arid4b*$^{+/-}$ bone marrow smears, original magnifications are the same). Five separate analyses were performed. Scale bars = 20 µm. **B**) Wright–Giemsa staining of peripheral blood smears from the AML *Arid4a*$^{-/-}$*Arid4b*$^{+/-}$ mice showing blasts (a, **black arrowhead**), lymphocytes (a, **white arrowhead**), increased numbers of immature cells (b–d, **arrowheads**), and phagocytosis of cells by a macrophage (e). Eight separate analyses were performed. Scale bars = 5 µm.

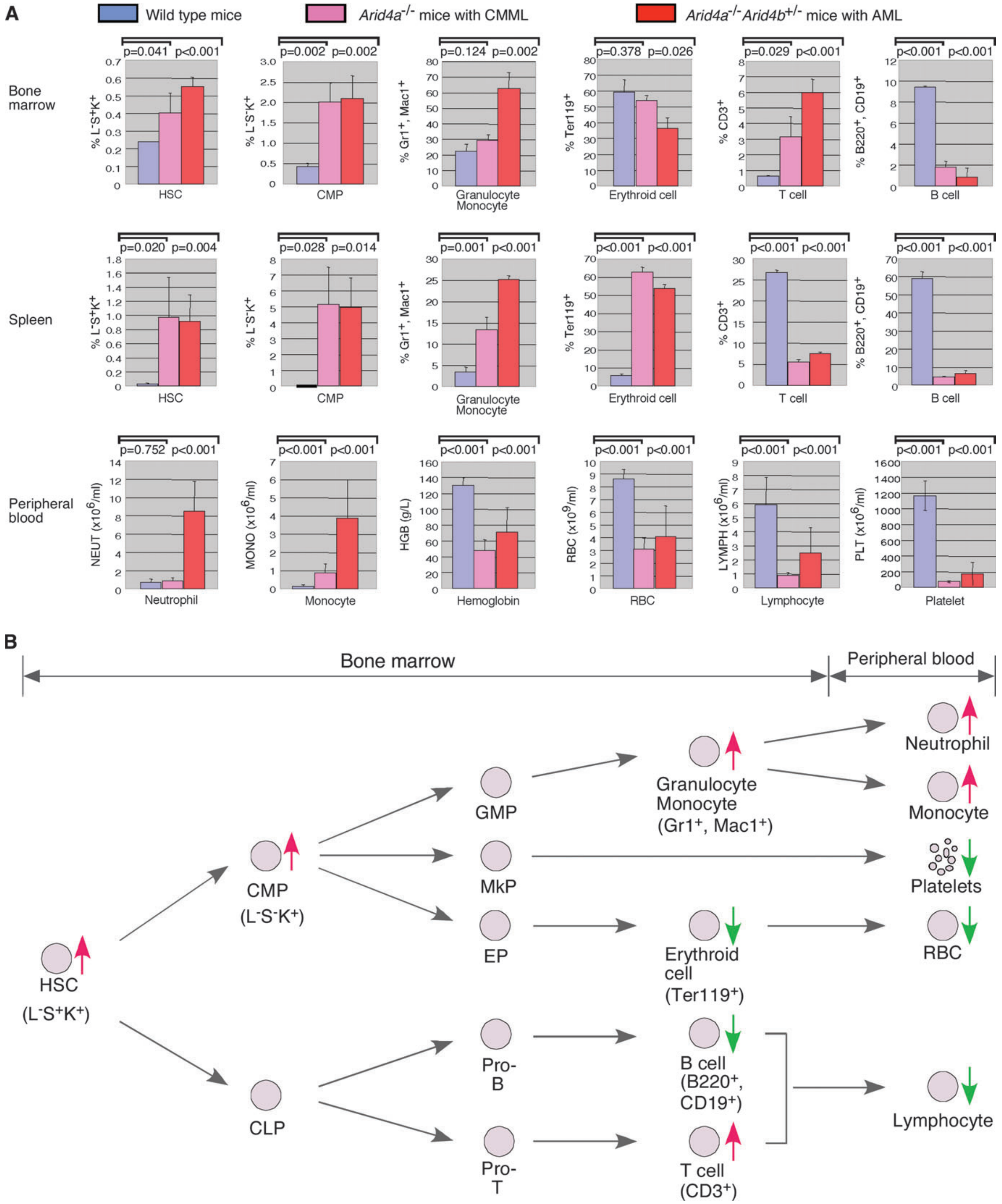

Figure 4. Hematopoietic lineage analysis of the *Arid4a*$^{-/-}$ mice and *Arid4a*$^{-/-}$*Arid4b*$^{+/-}$ leukemic mice. **A**) Comparison of cell populations in bone marrow and spleen (HSC, CMP, granulocyte, monocyte, erythroid cell, T cell, and B cell) and cell counts in peripheral blood (neutrophil, monocyte, hemoglobin, RBC, lymphocyte, and platelet) between wild-type mice (n = 5), the *Arid4a*$^{-/-}$ mice with CMML-like phenotype (n = 5), and the *Arid4a*$^{-/-}$*Arid4b*$^{+/-}$ mice with acute myeloid leukemia (AML) (n = 5). Means (and 95% confidence intervals) for all cell populations and cell counts are shown, and *P* values were calculated using Student *t* test. **B**) Hematopoietic lineage tree displaying the combined impact of the *Arid4a* mutation with or without the *Arid4b* mutations in bone marrow and peripheral blood of mice with CMML-like or AML phenotype. Increased and decreased cell populations are indicated by **red** and **green**, respectively. HSC, hematopoietc stem cell; CMP, common myeloid progenitor; CLP, common lymphoid progenitor; GMP, granulocyte and monocyte progenitor; MkP, megakaryocyte progenitor; EP, erythroid progenitor.

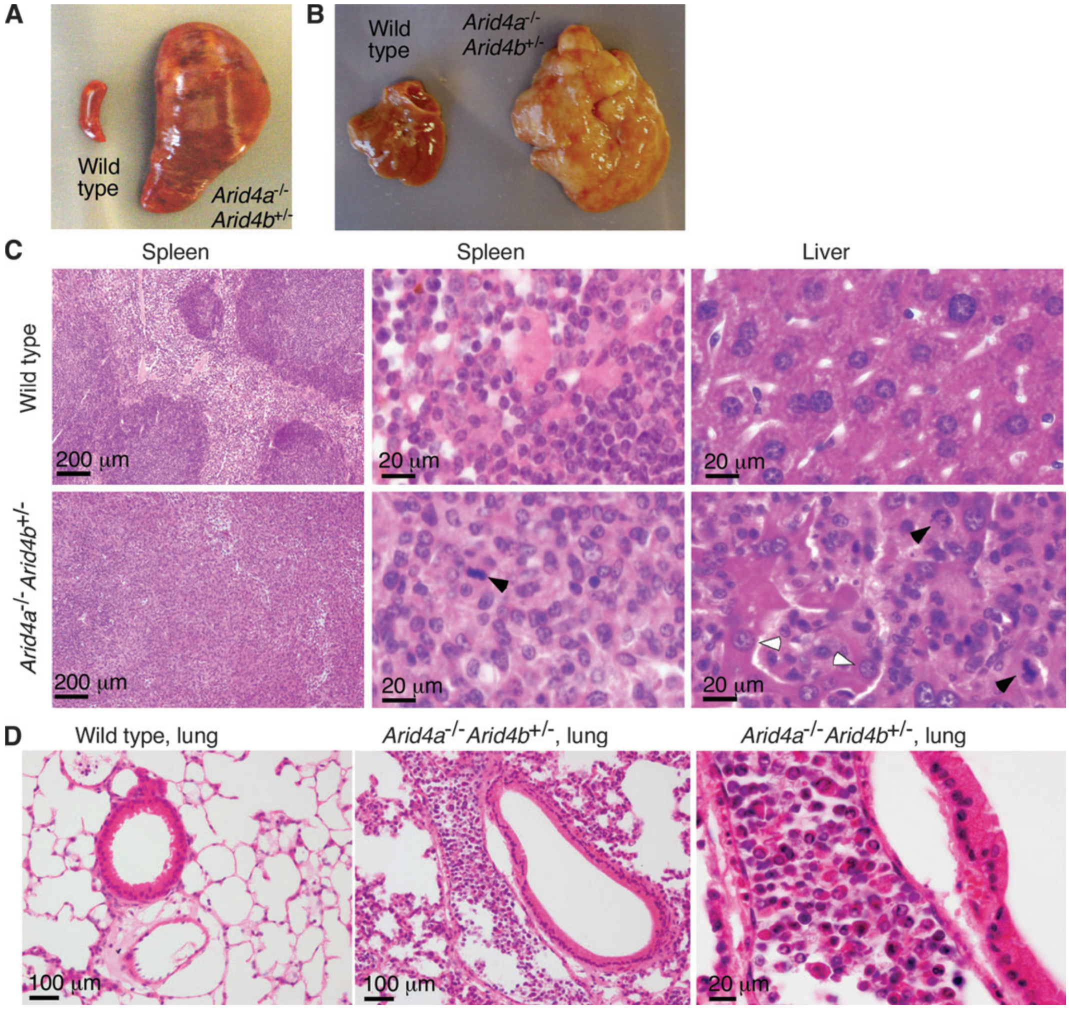

Figure 5. Development of myeloid sarcoma in *Arid4a*$^{-/-}$*Arid4b*$^{+/-}$ mice. **A**) Splenomegaly and **B**) hepatomegaly in the acute myeloid leukemia (AML) *Arid4a*$^{-/-}$*Arid4b*$^{+/-}$ mice relative to spleen and liver from wild-type littermates. **C**) Histologic analysis of spleen and liver from a wild-type mouse and an AML *Arid4a*$^{-/-}$*Arid4b*$^{+/-}$ mouse. Paraffin sections were stained with hematoxylin and eosin. **Black arrowheads** indicate mitotic leukemic cells in spleen and liver from the *Arid4a*$^{-/-}$*Arid4b*$^{+/-}$ mouse. **White arrowheads** indicate hepatocytes. **D**) Histologic analysis of lungs from a wild-type and an *Arid4a*$^{-/-}$ mouse. Paraffin sections were stained with hematoxylin and eosin. Blood vessels in the *Arid4a*$^{-/-}$ lungs showed a marked increase of leukemic cells.

(Figure 5, C). Blood vessels in the lungs of the AML mice showed a marked increase of nucleated elements, indicative of leukemic involvement (Figure 5, D). Similar lesions composed of leukemic cells were also found in lymph nodes and kidneys (data not shown). Flow cytometric analysis of cell populations within the splenic tissue showed an increase of leukocytes of granulocytic and monocytic origin (Gr1$^+$ and Mac1$^+$, 3% in wild-type mice, 13% in mice with CMML-like phenotype, and 26% in AML mice, difference between wild-type and CMML-like mice = 10%, $P < .001$; difference between wild-type and AML mice = 23%, $P < .001$) (Figure 4, A). This increase in granulocytes and monocytes was accompanied by an increase of erythroid cells (Ter119$^+$, 6% erythroid cells in wild-type mice, 63% in mice with CMML-like phenotype, and 54% in AML mice, difference between wild-type and CMML-like mice = 57%, $P < .001$; difference between wild-type and AML mice = 48%, $P < .001$) and relative decreases of the T lymphoid (CD3$^+$, 26.7% in wild-type mice, 5.5% in mice with CMML-like phenotype, and 7.6% in AML mice, difference between wild-type and CMML-like mice = 21.2%, $P < .001$; difference between wild-type and AML mice = 19.1%, $P < .001$) and B lymphoid (B220$^+$CD19$^+$, 58.9% in wild-type mice, 4.8% in mice with CMML-like phenotype, and 6.7% in AML mice, difference between wild-type and CMML-like mice = 54.1%, $P < .001$; difference between wild-type and AML mice = 52.2%, $P < .001$) populations (Figure 4, A). These features fulfill the criteria for AML (granulocytic and monocytic) and myeloid (granulocytic) sarcoma in mice (Bethesda proposals) (30).

Expansion of HSCs and Downstream Progenitors in *Arid4a*$^{-/-}$ and *Arid4a*$^{-/-}$*Arid4b*$^{+/-}$ Mice

Because the abnormalities were found in all hematologic lineages, we tested whether deficiency of *Arid4a* and *Arid4b* has effects on HSCs and downstream progenitors. Compared with wild-type mice, *Arid4a*$^{-/-}$ mice had an increased proportion of HSCs (Lin$^-$Sca1$^+$c-Kit$^+$, referred to as L$^-$S$^+$K$^+$, 0.24% in wild-type mice, 0.40% in *Arid4a*$^{-/-}$ mice, difference = 0.16%, $P = .041$) in bone marrow (Figure 4, A). In mice that were also heterozygous for the *Arid4b* mutation, there was greater expansion of the HSCs population in the *Arid4a*$^{-/-}$*Arid4b*$^{+/-}$ bone marrow ($L^-S^+K^+$, 0.24% in wild-type mice, 0.55% in *Arid4a*$^{-/-}$*Arid4b*$^{+/-}$ mice, difference = 0.31%, $P < .001$) (Figure 4, A). Furthermore, the proportions of CMPs ($Lin^-Sca1^-c\text{-}Kit^+$, referred as $L^-S^-K^+$) in the *Arid4a*$^{-/-}$ and *Arid4a*$^{-/-}$*Arid4b*$^{+/-}$ bone marrow were statistically significantly higher than those from wild-type mice ($L^-S^-K^+$, 0.4% in wild-type mice, 2.0% in mice with CMML-like phenotype, and 2.1% in AML mice, difference between wild-type and CMML-like mice = 1.6%, $P < .001$; difference between wild-type and AML mice = 1.7%, $P < .001$) (Figure 4, A). In the spleen, dramatic increases of the HSC ($L^-S^+K^+$, 0.03% in wild-type mice, 0.4% in mice with CMML-like phenotype, and 0.55% in AML mice, difference between wild-type and CMML-like mice = 0.37%, $P = .02$; difference between wild-type and AML mice = 0.52%, $P = .004$) and CMP ($L^-S^-K^+$, 0.01% in wild-type mice, 5.13% in mice with CMML-like phenotype, and 5.01% in AML mice, difference between wild-type and CMML-like mice = 5.12%, $P = .028$; difference between wild-type and AML mice = 5%, $P = .014$) populations were found in both *Arid4a*$^{-/-}$ mice and *Arid4a*$^{-/-}$*Arid4b*$^{+/-}$ mice (Figure 4, A), suggesting that extramedullary hematopoiesis in spleen might be due to mobilization of HSCs from bone marrow.

Collectively, our data suggested the following disease model for the observed hematologic disorders. Deficiency of *Arid4a* and *Arid4b* results in increase of HSCs, CMPs, and $Gr1^+Mac1^+$ myeloid cells in bone marrow and spleen, which leads to increases of neutrophils and monocytes in the peripheral blood (Figure 4, B). Despite the compensatory erythropoiesis within the enlarged spleen due to the decrease of erythroid activity in the bone marrow (Figures 1, J and 4, A and B), the enlarged spleen sequestrates RBCs. Although it is not known if the reduction in platelets is due to decreased production or increased destruction, the reduction leads to spontaneous hemorrhage (Supplementary Figure 1, available online). All of these processes contribute to a decrease of RBCs in peripheral blood (Figure 4, B). Although the proportion of T lymphoid cells was increased in the bone marrow, the population of B lymphoid cells was substantially decreased, leading to the lower number of total lymphocytes in the peripheral blood (Figure 4, B). Thus, *Arid4a* and *Arid4b* have essential roles in hematopoietic homeostasis and in lineage fate determination.

Disturbed Patterns of Histone Modifications in *Arid4a*$^{-/-}$ Bone Marrow Cells

The ARID4A and ARID4B proteins contain a chromodomain and a Tudor domain. Both domains have been reported to mediate binding to methylated lysines of histones H3 and H4 (11–14). Given the bone marrow failure phenotype found in the *Arid4a*$^{-/-}$ mice, we investigated the expression and methylation status of histones in bone marrow of these mice. By western blot analysis, levels of histones H3 and H4 were elevated by 2.7- and 2.2-fold, respectively (95% CI = 2.3 to 3.1 and 1.9 to 2.5, respectively) in the *Arid4a*$^{-/-}$ bone marrow constituents compared with the wild-type samples (Figure 6, A). Levels of H2AX were not different. Methylation of lysine in H3 can lead to either repression or activation of gene expression; trimethylation of H3K4 (H3K4me3) is associated with transcriptional activation at euchromatic regions, whereas trimethylation of H3K9 (H3K9me3) is usually associated with repressive states at pericentric heterochromatin. Analysis of H3 lysine methylation revealed very large increases of both H3K4me3 (32-fold, 95% CI = 27 to 37) and H3K9me3 (45-fold, 95% CI = 41 to 49) in the bone marrow cells from the *Arid4a*$^{-/-}$ mice compared with wild-type mice (Figure 6, A). As detected by immunofluorescence, H3K4me3 was broadly distributed over euchromatic regions but showed speckled patterns in both wild-type and *Arid4a*$^{-/-}$ bone marrow cells (Figure 6, B). In wild-type bone marrow cells, H3K9me3 was localized in discrete spots in the DAPI-dense regions that correspond to the pericentric heterochromatin structure (Figure 6, B). *Arid4a*$^{-/-}$ bone marrow cells showed a diffuse pattern of H3K9me3-derived immunofluorescence with small foci spread throughout the nuclei (Figure 6, B). These different patterns of H3K9me3 between wild-type and the *Arid4a*$^{-/-}$ samples were obvious across the great majority of cells in the marrow even though the cell populations in wild-type and the *Arid4a*$^{-/-}$ bone marrow samples were different (Figure 4, A). These differences of immunofluorescence staining patterns of H3K9me3 were not seen in primary mouse embryo fibroblasts (pMEFs) (Figure 6, B). Trimethylation of H4K20 (H4K20me3) is another modification usually found on repressed chromatin accumulated at pericentric heterochromatin regions. When analyzed by western blotting, the *Arid4a*$^{-/-}$ bone marrow cells revealed a slight increase of H4K20me3 (2.2-fold, 95% CI = 1.7 to 2.7), which might reflect increased expression of histone H4 (2.2-fold, 95% CI = 1.9 to 2.5) (Figure 6, A). The fluorescence signals representing H4K20me3 were focally enriched at pericentric heterochromatin in both wild-type and the *Arid4a*$^{-/-}$ bone marrow cells (Figure 6, B). Collectively, these results suggest that *Arid4a* participates in regulating lysine trimethylation of histones H3 and H4 in bone marrow.

Decreased Expression of the *Hox* and *Fox* Genes in Bone Marrow Cells with *Arid4a* and *Arid4b*$^{+/-}$ Mutations

To investigate the downstream genes regulated by *Arid4a* and *Arid4b*, we first compared gene expression of wild-type pMEFs and *Arid4a*$^{-/-}$*Arid4b*$^{+/-}$ pMEFs using gene expression microarrays. We identified genotype-specific differences in expression of *Hox* and *Fox* genes (data not shown). To further elucidate the regulatory mechanisms by which *Arid4a* and *Arid4b* are involved in acquisition of the leukemic phenotype, we compared expression of several genes important for normal hematopoiesis and leukemogenesis. These included the homeobox genes in the *Hox* clusters (*Hoxa*, *Hoxb*, and *Hoxc*) (31,32), homeodomain transcription factors *Pbx1* (33), *Meis1* (34), and *Pitx2* (35), *AML1* (acute myeloid leukemia 1) (36), *Mll* (mixed-lineage leukemia) (37), and the forkhead box gene *Foxp3* (38,39). We compared the expression of these genes in bone marrow from wild-type, *Arid4a*$^{-/-}$, and *Arid4a*$^{-/-}$*Arid4b*$^{+/-}$ mice. To minimize variation arising from differences in cell populations, we collected bone marrow cells from mice before development of illness. We monitored relative gene expression levels using reverse transcription–PCR. The expression of several *Hoxb* genes, including *Hoxb3*, *Hoxb5*, *Hoxb6*, and *Hoxb8*, but not *Hoxb4*, was decreased in both *Arid4a*$^{-/-}$ and *Arid4a*$^{-/-}$*Arid4b*$^{+/-}$ bone marrow compared to wild-type mice. This decrease was specific for *Hoxb* genes because the expression of *Hoxa7*, *Hoxa9*, *Hoxc6*, *Pbx1*, and *Meis1* was not altered (Figure 7, A). The expression of *Pitx2* that is required for normal hematopoiesis was also reduced in *Arid4a*$^{-/-}$ and *Arid4a*$^{-/-}$*Arid4b*$^{+/-}$ bone marrow (Figure 7, A). In contrast, expression of

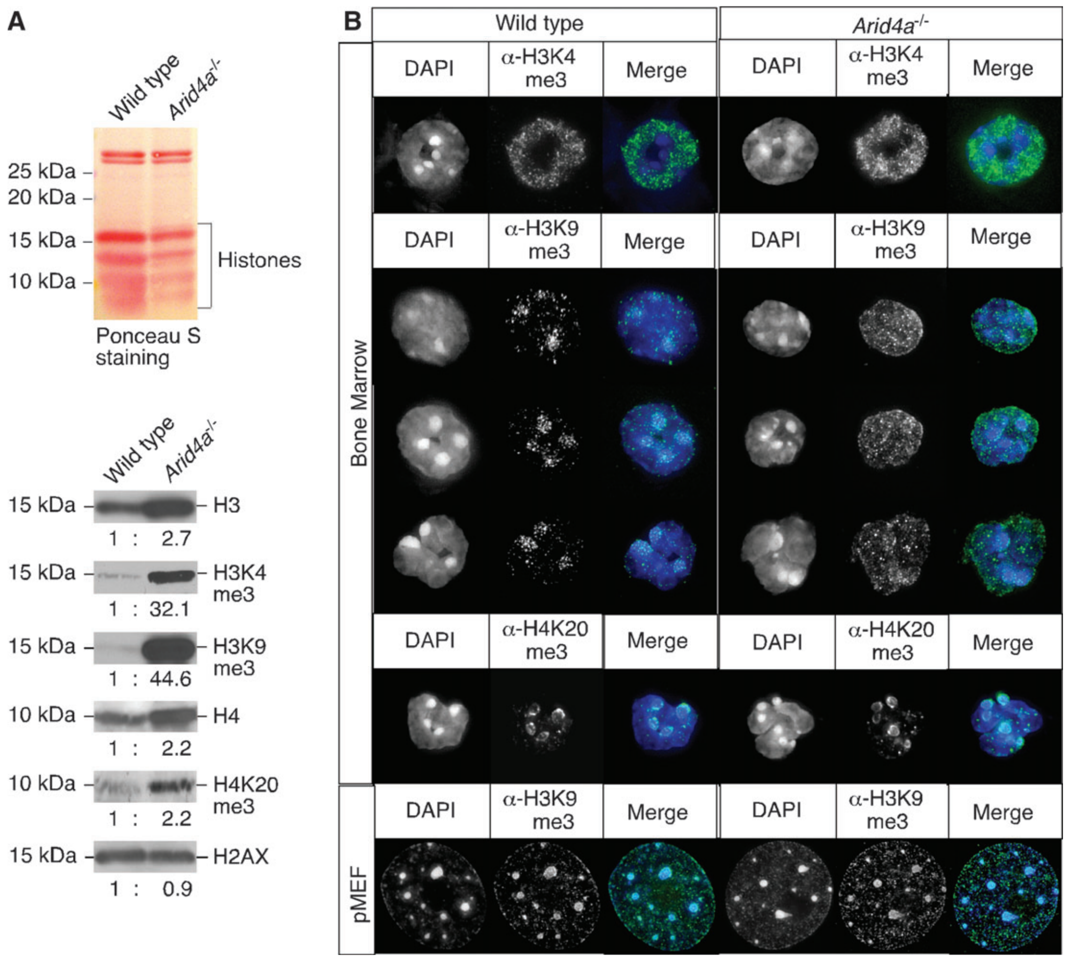

Figure 6. Histone modifications in bone marrow cells of mice lacking *Arid4a*. **A**) Western blot analysis of acid-extracted proteins from bone marrow of a wild-type and an *Arid4a*$^{-/-}$ mouse. Total proteins were transferred to a nitrocellulose membrane and stained with Ponceau S (top), followed by staining with antibodies against histones H3, H4, H2AX, H3K4me3, H3K9me3, and H4K20me3 (bottom). Ratios of histones were quantified by densitometry. Five separate experiments were performed. **B**) Immunofluorescence analysis of bone marrow cells or primary mouse embryo fibroblasts from wild-type and the *Arid4a*$^{-/-}$ mice using antibodies against H3K4me3, H3K9me3, and H4K20me3. DNA was counterstained with DAPI. Images were analyzed by deconvolution microscopy. Three separate experiments were performed, all with similar results.

AML1 and *Mll*, genes involved in leukemogenesis, was similar in all the bone marrow samples (Figure 7, A). These results suggested that *Arid4a* regulates hematopoiesis by controlling the expression of specific homeodomain genes, such as *Pitx2* and a subset of *Hoxb* genes.

The FOXP3 protein plays an important role in control of the regulatory T-cell lineage (40), and *Foxp3* was recently identified as a tumor suppressor gene (41). The expression of *Foxp3* was reduced specifically in the *Arid4a*$^{-/-}$*Arid4b*$^{+/-}$ bone marrow but not in the *Arid4a*$^{-/-}$ bone marrow (Figure 7, A), suggesting that downregulation of *Foxp3* may be involved in the mechanisms underlying the increased numbers of T cells in the *Arid4a*$^{-/-}$*Arid4b*$^{+/-}$ bone marrow (Figure 4, A) and the high frequency of leukemia malignancies in the *Arid4a*$^{-/-}$*Arid4b*$^{+/-}$ mice.

Discussion

Arid4a and *Arid4b* knockout mice provide a suitable animal model for better understanding the progression of a premalignant hematologic disorder and the eventual transformation to AML. Using this model, we found disruption of myeloid homeostasis in the *Arid4a*$^{-/-}$ mice due to the increase of HSCs and downstream progenitors, which might be the principal components of the expansion of a transformed leukemic stem cell compartment with aggressive self-renewal properties. We have obtained some insight into the molecular mechanisms by defining the downstream regulatory impact on the *Hox* and *Fox* genes. Moreover, our results suggest that *Arid4a* controls chromatin modification necessary to support normal hematopoiesis, and the data are consistent with an important role of epigenetic regulation in cancer development.

H3K4me3 is a mark of transcriptionally active chromatin states, whereas the H3K9me3 and H4K20me3 modifications are usually found at repressive chromatin domains. However, we found that H3K4me3, H3K9me3, and H4K20me3 were all increased in bone marrow cells from mice deleted for *Arid4a*. We envision that these histone methylations will reach a combinatorial steady state that may mediate activation or repression of specific genomic loci or chromosome domains. We propose that ARID4A is a critical determinant for distinct histone methylation states and that it plays

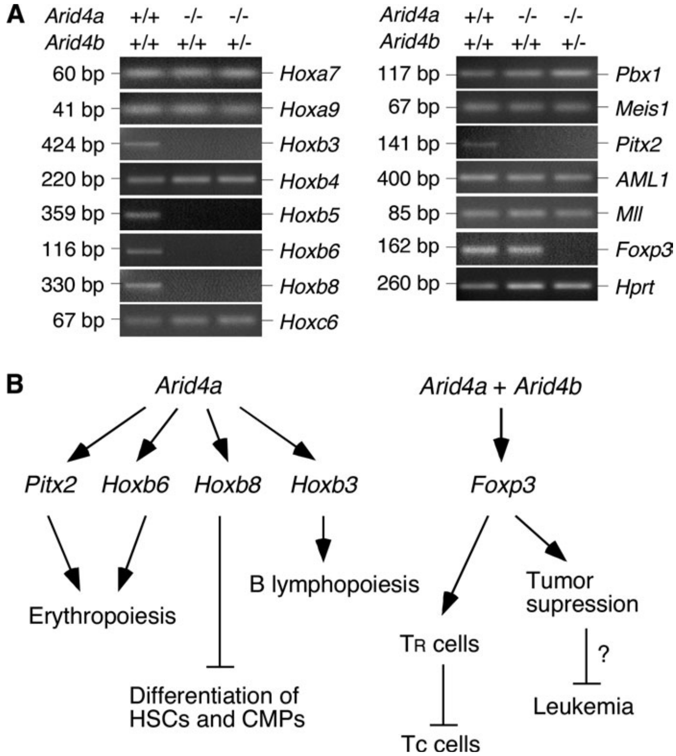

Figure 7. Gene expression analysis of bone marrow cells from wild-type, *Arid4a*$^{-/-}$, and *Arid4a*$^{-/-}$*Arid4b*$^{+/-}$ mice. **A**) Reverse transcriptase–polymerase chain reaction was performed to analyze the genes indicated, with *Hprt* serving as the control gene. Three separate experiments were performed. **B**) Pathways by which *Arid4a* and *Arid4b* might regulate hematopoiesis through control of the *Hox* and *Fox* genes. In the scenario shown, *Arid4a* controls erythropoiesis, possibly by positively regulating *Pitx2* and *Hoxb6* genes. *Arid4a* also controls the expression of *Hoxb8*, whose product blocks differentiation of hematopoietic stem cells and common myeloid progenitors. Control of B lymphopoiesis by *Arid4a* may be achieved by increasing expression of *Hoxb3*. *Arid4a*, together with *Arid4b*, increases expression of *Foxp3*, which acts on regulatory T (TR) cells to suppress conventional T (Tc) cells. *Foxp3* also functions as a tumor suppressor gene. However, it is unclear whether *Foxp3* suppresses leukemia malignancies.

an important role in coordination between the modification marks at different chromatin regions. Further analysis of chromatin-specific components associated with ARID4A and/or ARID4B could more clearly address the contribution of these two proteins to the combinatorial pattern of histone modifications. A goal of future research should be to determine whether ARID4A and ARID4B contain any intrinsic enzyme activity and whether they mediate their effects either through direct interaction with chromatin complexes or through intermediate steps involving various pathways that are modulated through chromatin remodeling.

Our results suggest plausible molecular mechanisms for the hematologic disorder in *Arid4a*-deficient mice based on downregulation of a number of homeobox genes (*Pitx2* and a cluster of *Hoxb* genes including *Hoxb3*, *Hoxb5*, *Hoxb6*, and *Hoxb8*) in *Arid4a*$^{-/-}$ bone marrow cells with or without *Arid4b* haploinsufficiency. A homeobox sequence encodes a protein domain that binds DNA. Homeobox genes encode transcription factors and are classified into two subgroups: Hox and non–Hox genes. Abnormal expression of both groups of homeobox genes plays a role in the pathogenesis of myeloid malignancies (31,32). Little is known about the molecular mechanisms of homeobox gene regulation, but the *MLL* gene is reported to positively regulate multiple *Hox* genes (28). *MLL* encodes a histone methyltransferase that methylates H3K4 (42). Leukemogenic *MLL* translocations define a specific group of leukemias (mixed lineage leukemia) (43). We suggest that *Arid4a* and *Arid4b* play a prominent role in leukemic transformation by controlling the trimethylation of H3K4 and H3K9. Although we did not find that mutations of *Arid4a* and *Arid4b* affected the expression of *Mll*, our results suggest plausible molecular mechanisms whereby *Arid4a* and *Arid4b* might regulate hematopoiesis by controlling the expression of specific homeodomain genes, such as *Pitx2*, required for normal erythropoiesis (44), and a subset of *Hoxb* genes, including *Hoxb6*, whose disruption results in an increase of early erythrocyte progenitors (45); *Hoxb*8, which affects lineage-specific development of hematopoietic progenitor cells (46,47); and *Hoxb3*, whose deficiency impairs B lymphopoiesis (48) (Figure 7, B).

Our results also imply that *Arid4a* and *Arid4b* are involved in the regulation of a forkhead box gene *Foxp3* (Figure 7, B), an X chromosome–encoded forkhead transcription factor family member that plays an important role in the development and function of natural regulatory T cells (40). FOXP3 protein interacts with AML1 to control regulatory T-cell function (39). Although *Arid4a* and *Arid4b* mutations did not affect the expression of *AML1*, we found decreased expression of *Foxp3* in the *Arid4a*$^{-/-}$*Arid4b*$^{+/-}$ mice. FOXP3 functions as a transcriptional regulator by assembling chromatin remodeling complexes involved in histone modification (49). In humans, mutations of *FOXP3* leads to an X-linked fatal autoimmune disease known as IPEX (immune dysregulation, polyendocrinopathy, enteropathy, X-linked) syndrome and an analogous lymphoproliferative disease (50). Deficiency of *Foxp3* in mice leads to an early onset, highly aggressive and fatal autoimmune disease characterized by excessive proliferation of CD4^{+} T cells and extensive infiltration by leukocytes in multiple organs (38,51,52). Recently, it has been reported that FOXP3 protein functions as a tumor suppressor involved in the development of breast cancer (41). Decreased expression of *Foxp3* may be involved in the disease mechanisms through epigenetic effects in the *Arid4a*$^{-/-}$*Arid4b*$^{+/-}$ mice, which develop an increased population of T cells in bone marrow and progress to AML and myeloid sarcoma with various tissues infiltrated by leukemic cells. It will be of interest to examine whether decreased expression of *Foxp3* contributes to the high frequency of leukemia malignancies in the *Arid4a*$^{-/-}$*Arid4b*$^{+/-}$ mice.

We present evidence that ARID4A and ARID4B function as tumor suppressors and that a myelodysplastic/myeloproliferative disorder in mice carrying the *Arid4a* or/and *Arid4b* mutations progresses to hematologic malignancies, resembling human CMML and AML. However, we have not investigated whether mutations in *ARID4A* and *ARID4B* participate in genetic and/or epigenetic mechanisms of human CMML and AML, or other cancers. Although the ARID4A and ARID4B proteins have been identified as breast cancer–associated antigens (3,20,21) and *Arid4a* and *Arid4b* are involved in the regulation of *Foxp3*, which functions as a breast cancer suppressor gene (41), we have not observed primary solid tumors in mice with ARID4 family deficiency, (although we have not performed a detailed search for breast cancer). Further study of the *Arid4* gene family may advance our understanding of the connection between gene regulation, epigenetic control, disease development, and cancer formation. We also suggest that gene regulation by ARID4A and ARID4B should be examined for potential disease-related roles, not only in human malignancies, but also in other complex disease traits.

References

1. Defeo-Jones D, Huang PS, Jones RE, et al. Cloning of cDNAs for cellular proteins that bind to the retinoblastoma gene product. *Nature*. 1991; 352(6332):251–254.
2. Fattaey AR, Helin K, Dembski MS, et al. Characterization of the retinoblastoma binding proteins RBP1 and RBP2. *Oncogene*. 1993;8(11):3149–3156.
3. Cao J, Gao T, Stanbridge EJ, Irie R. RBP1L1, a retinoblastoma-binding protein-related gene encoding an antigenic epitope abundantly expressed in human carcinomas and normal testis. *J Natl Cancer Inst*. 2001;93(15): 1159–1165.
4. Wilsker D, Probst L, Wain HM, Maltais L, Tucker PW, Moran E. Nomenclature of the ARID family of DNA-binding proteins. *Genomics*. 2005;86(2):242–251.
5. Wu MY, Tsai TF, Beaudet AL. Deficiency of Rbbp1/Arid4a and Rbbp1l1/Arid4b alters epigenetic modifications and suppresses an imprinting defect in the PWS/AS domain. *Genes Dev*. 2006;20(20):2859–2870.
6. Lai A, Lee JM, Yang WM, et al. RBP1 recruits both histone deacetylase-dependent and -independent repression activities to retinoblastoma family proteins. *Mol Cell Biol*. 1999;19(10):6632–6641.
7. Patsialou A, Wilsker D, Moran E. DNA-binding properties of ARID family proteins. *Nucleic Acids Res*. 2005;33(1):66–80.
8. Bannister AJ, Zegerman P, Partridge JF, et al. Selective recognition of methylated lysine 9 on histone H3 by the HP1 chromo domain. *Nature*. 2001;410(6824):120–124.
9. Fischle W, Wang Y, Jacobs SA, Kim Y, Allis CD, Khorasanizadeh S. Molecular basis for the discrimination of repressive methyl-lysine marks in histone H3 by Polycomb and HP1 chromodomains. *Genes Dev*. 2003; 17(15):1870–1881.
10. Pray-Grant MG, Daniel JA, Schieltz D, Yates JR III, Grant PA. Chd1 chromodomain links histone H3 methylation with SAGA- and SLIK-dependent acetylation. *Nature*. 2005;433(7024):434–438.
11. Lachner M, O'Carroll D, Rea S, Mechtler K, Jenuwein T. Methylation of histone H3 lysine 9 creates a binding site for HP1 proteins. *Nature*. 2001;410(6824):116–120.
12. Min J, Zhang Y, Xu RM. Structural basis for specific binding of Polycomb chromodomain to histone H3 methylated at Lys 27. *Genes Dev*. 2003;17(15):1823–1828.
13. Sanders SL, Portoso M, Mata J, Bahler J, Allshire RC, Kouzarides T. Methylation of histone H4 lysine 20 controls recruitment of Crb2 to sites of DNA damage. *Cell*. 2004;119(5):603–614.
14. Huang Y, Fang J, Bedford MT, Zhang Y, Xu RM. Recognition of histone H3 lysine-4 methylation by the double tudor domain of JMJD2A. *Science*. 2006;312(5774):748–751.
15. Lai A, Marcellus RC, Corbeil HB, Branton PE. RBP1 induces growth arrest by repression of E2F-dependent transcription. *Oncogene*. 1999;18(12): 2091–2100.
16. Lai A, Kennedy BK, Barbie DA, et al. RBP1 recruits the mSIN3-histone deacetylase complex to the pocket of retinoblastoma tumor suppressor family proteins found in limited discrete regions of the nucleus at growth arrest. *Mol Cell Biol*. 2001;21(8):2918–2932.
17. Fleischer TC, Yun UJ, Ayer DE. Identification and characterization of three new components of the mSin3A corepressor complex. *Mol Cell Biol*. 2003;23(10):3456–3467.
18. Binda O, Roy JS, Branton PE. RBP1 family proteins exhibit SUMOylation-dependent transcriptional repression and induce cell growth inhibition reminiscent of senescence. *Mol Cell Biol*. 2006;26(5): 1917–1931.
19. Classon M, Harlow E. The retinoblastoma tumour suppressor in development and cancer. *Nat Rev Cancer*. 2002;2(12):910–917.
20. Cao J, Gao T, Giuliano AE, Irie RF. Recognition of an epitope of a breast cancer antigen by human antibody. *Breast Cancer Res Treat*. 1999;53(3): 279–290.
21. Cui D, Jin G, Gao T, et al. Characterization of BRCAA1 and its novel antigen epitope identification. *Cancer Epidemiol Biomarkers Prev*. 2004;13(7):1136–1145.
22. Takahashi T, Cao J, Hoon DS, Irie RF. Cytotoxic T lymphocytes that recognize decameric peptide sequences of retinoblastoma binding protein 1 (RBP-1) associated with human breast cancer. *Br J Cancer*. 1999;81(2):342–349.
23. Meehan WJ, Samant RS, Hopper JE, et al. Breast cancer metastasis suppressor 1 (BRMS1) forms complexes with retinoblastoma-binding protein 1 (RBP1) and the mSin3 histone deacetylase complex and represses transcription. *J Biol Chem*. 2004;279(2):1562–1569.
24. Nikolaev AY, Papanikolaou NA, Li M, Qin J, Gu W. Identification of a novel BRMS1-homologue protein p40 as a component of the mSin3A/p33(ING1b)/HDAC1 deacetylase complex. *Biochem Biophys Res Commun*. 2004;323(4):1216–1222.
25. Seraj MJ, Samant RS, Verderame MF, Welch DR. Functional evidence for a novel human breast carcinoma metastasis suppressor, BRMS1, encoded at chromosome 11q13. *Cancer Res*. 2000;60(11):2764–2769.
26. Wang GG, Allis CD, Chi P. Chromatin remodeling and cancer, part I: covalent histone modifications. *Trends Mol Med*. 2007;13(9):363–372.
27. Miremadi A, Oestergaard MZ, Pharoah PD, Caldas C. Cancer genetics of epigenetic genes. *Hum Mol Genet*. 2007;16 Spec No. 1:R28–R49.
28. Ernst P, Mabon M, Davidson AJ, Zon LI, Korsmeyer SJ. An Mll-dependent Hox program drives hematopoietic progenitor expansion. *Curr Biol*. 2004; 14(22):2063–2069.
29. Vardiman JW, Harris NL, Brunning RD. The World Health Organization (WHO) classification of the myeloid neoplasms. *Blood*. 2002;100(7): 2292–2302.
30. Kogan SC, Ward JM, Anver MR, et al. Bethesda proposals for classification of nonlymphoid hematopoietic neoplasms in mice. *Blood*. 2002;100(1):238–245.
31. Eklund EA. The role of HOX genes in malignant myeloid disease. *Curr Opin Hematol*. 2007;14(2):85–89.
32. Rice KL, Licht JD. HOX deregulation in acute myeloid leukemia. *J Clin Invest*. 2007;117(4):865–868.
33. Kamps MP, Baltimore D. E2A-Pbx1, the t(1;19) translocation protein of human pre-B-cell acute lymphocytic leukemia, causes acute myeloid leukemia in mice. *Mol Cell Biol*. 1993;13(1):351–357.
34. Moskow JJ, Bullrich F, Huebner K, Daar IO, Buchberg AM. Meis1, a PBX1-related homeobox gene involved in myeloid leukemia in BXH-2 mice. *Mol Cell Biol*. 1995;15(10):5434–5443.
35. Arakawa H, Nakamura T, Zhadanov AB, et al. Identification and characterization of the ARP1 gene, a target for the human acute leukemia ALL1 gene. *Proc Natl Acad Sci USA*. 1998;95(8):4573–4578.
36. Miyoshi H, Shimizu K, Kozu T, Maseki N, Kaneko Y, Ohki M. t(8;21) breakpoints on chromosome 21 in acute myeloid leukemia are clustered within a limited region of a single gene, AML1. *Proc Natl Acad Sci USA*. 1991;88(23):10431–10434.
37. Ziemin-van der Poel S, McCabe NR, Gill HJ, et al. Identification of a gene, MLL, that spans the breakpoint in 11q23 translocations associated with human leukemias. *Proc Natl Acad Sci USA*. 1991;88(23):10735–10739.
38. Brunkow ME, Jeffery EW, Hjerrild KA, et al. Disruption of a new forkhead/winged-helix protein, scurfin, results in the fatal lymphoproliferative disorder of the scurfy mouse. *Nat Genet*. 2001;27(1):68–73.
39. Ono M, Yaguchi H, Ohkura N, et al. Foxp3 controls regulatory T-cell function by interacting with AML1/Runx1. *Nature*. 2007;446(7136):685–689.
40. Zheng Y, Rudensky AY. Foxp3 in control of the regulatory T cell lineage. *Nat Immunol*. 2007;8(5):457–462.
41. Zuo T, Wang L, Morrison C, et al. FOXP3 is an X-linked breast cancer suppressor gene and an important repressor of the HER-2/ErbB2 oncogene. *Cell*. 2007;129(7):1275–1286.
42. Milne TA, Briggs SD, Brock HW, et al. MLL targets SET domain methyltransferase activity to Hox gene promoters. *Mol Cell*. 2002;10(5): 1107–1117.
43. Huret JL, Dessen P, Bernheim A. An atlas of chromosomes in hematological malignancies. Example: 11q23 and MLL partners. *Leukemia*. 2001; 15(6):987–989.
44. Zhang HZ, Degar BA, Rogoulina S, et al. Hematopoiesis following disruption of the Pitx2 homeodomain gene. *Exp Hematol*. 2006;34(2):167–178.

45. Kappen C. Disruption of the homeobox gene Hoxb-6 in mice results in increased numbers of early erythrocyte progenitors. *Am J Hematol.* 2000; 65(2):111–118.
46. Krishnaraju K, Hoffman B, Liebermann DA. Lineage-specific regulation of hematopoiesis by HOX-B8 (HOX-2.4): inhibition of granulocytic differentiation and potentiation of monocytic differentiation. *Blood.* 1997;90(5):1840–1849.
47. Knoepfler PS, Sykes DB, Pasillas M, Kamps MP. HoxB8 requires its Pbx-interaction motif to block differentiation of primary myeloid progenitors and of most cell line models of myeloid differentiation. *Oncogene.* 2001; 20(39):5440–5448.
48. Bjornsson JM, Larsson N, Brun AC, et al. Reduced proliferative capacity of hematopoietic stem cells deficient in Hoxb3 and Hoxb4. *Mol Cell Biol.* 2003;23(11):3872–3883.
49. Li B, Saouaf SJ, Samanta A, Shen Y, Hancock WW, Greene MI. Biochemistry and therapeutic implications of mechanisms involved in FOXP3 activity in immune suppression. *Curr Opin Immunol.* 2007; 19(5):583–588.
50. Chatila TA, Blaeser F, Ho N, et al. JM2, encoding a fork head-related protein, is mutated in X-linked autoimmunity-allergic disregulation syndrome. *J Clin Invest.* 2000;106(12):R75–R81.
51. Bennett CL, Christie J, Ramsdell F, et al. The immune dysregulation, polyendocrinopathy, enteropathy, X-linked syndrome (IPEX) is caused by mutations of FOXP3. *Nat Genet.* 2001;27(1):20–21.
52. Wildin RS, Ramsdell F, Peake J, et al. X-linked neonatal diabetes mellitus, enteropathy and endocrinopathy syndrome is the human equivalent of mouse scurfy. *Nat Genet.* 2001;27(1):18–20.

Funding

National Institutes of Health (HD-37283 to A.L.B.).

Notes

We are particularly grateful to Silvia Briones, Catherine Tran, and Minnie Freeman for technical assistance. We thank Ray-Chang Wu, Orla M. Conneely, Shuo Zhang, Alice J. Chen, Stuart M. Chambers, and Neal Copeland for critical reading of the manuscript.

The sponsor had no role in the study design, data collection and analysis, interpretation of the results, the preparation of the manuscript, or the decision to submit the manuscript for publication.

The authors declare no competing financial interests.

Manuscript received January 25, 2008; revised May 13, 2008; accepted June 19, 2008.